EuroIntervention 2012;8:511-519 published online ahead of print May 2012

Non-invasive fractional flow reserve: scientific basis, methods and perspectives

Patrick W. Serruys*, MD, PhD; Chrysafios Girasis, MD; Stella-Lida Papadopoulou, MD; Yoshinobu Onuma, MD

Thoraxcenter, Erasmus MC, Rotterdam, The Netherlands

This paper also includes accompanying supplementary data published at the following website: www.eurointervention.org

Introduction

In 2008, our group investigated the accuracy of quantitative measurements for lumen, vessel and plaque volume derived from multislice computed tomography (MSCT) scans in comparison with intravascular ultrasound (IVUS) greyscale in a cohort of 47 patients: an excellent correlation and a relatively acceptable agreement were shown[1]. More recently, Voros and colleagues reviewed the field and published a comprehensive analysis of the relationship between MSCT- and IVUS-derived measures for lumen and plaque area[2]. They concluded that for lumen and vessel areas good correlations exist with a coefficient higher than 0.7, and a systematic error of about 20%, MSCT values being consistently overestimated. Regarding percentage of atheroma volume, the correlation was only modest with a coefficient of correlation close to 0.5, and in general the Bland-Altman plot showed an acceptable mean difference though with relatively wide limits of agreement. The same authors also reviewed the capability of MSCT to characterise tissues, using the classical threshold of more than 150 Hounsfield units (HU) for calcified plaque, 30-149 HU for high-density non-calcified plaque, and -100 to 30 HU for low-density non-calcified plaque. Only a modest correlation was found for both calcified and non-calcified plaque area, and both components were excessively overestimated by CT angiography (CTA) with rather poor overall agreement. In the authors' experience, high-density non-calcified plaque as quantified by MSCT had a closer, even if moderate, correlation with the percentage of fibrous tissue derived by IVUS virtual histology (IVUS-VH), whereas only a poor correlation existed between low-density non-calcified plaque and fibro-fatty tissue plus necrotic core. This component was apparently underestimated by CTA.

One of the intrinsic limitations of CTA in assessing plaque characteristics is the fact that the contrast density of the lumen impacts on the plaque density in the surroundings of the lumen. For instance, a plaque characterised as fibrous with 100 HU at the time of the peak contrast filling of the lumen (e.g., a density of 330 HU) could appear like a lipid plaque with 30 HU as soon as the contrast medium and its density are cleared out of the vessel lumen[3,4] **(Figure 1)**. Despite this limitation, vendors have created software algorithms which can differentiate between diverse types of tissue based on MSCT[2,5-7]. More recently, a fusion of near-infrared spectroscopy combined with IVUS and MSCT has provided *in vivo* three-dimensional (3D) distribution of lipid-core plaque in human coronary arteries[8].

Beyond luminography and tissue characterisation, MSCT has so far been unable to provide a functional assessment of the severity of epicardial narrowings. Over the last 15 years, research in the field

*Corresponding author: Thoraxcenter, Ba-583, 's Gravendijkwal 230, 3015 CE Rotterdam, The Netherlands.
E-mail: p.w.j.c.serruys@erasmusmc.nl

DOI: 10.4244/EIJV8I4A79

has made major progress and some landmark discoveries, such as the introduction and validation of patient-specific 3D blood flow analysis, the development of adaptive finite element models for simulating cardiovascular blood flow, the definition of physiologically realistic inflow and outflow boundary conditions as well as the coupled description of blood flow and vessel wall dynamics. Recently, methods for modelling coronary artery flow and auto-regulatory mechanisms have also been developed **(Table 1)**.

Our group has actively participated in this line of research: in 2000, we published the true 3D reconstruction of coronary arteries in patients by fusion of angiography and IVUS, and quantitatively validated this method[9]. In parallel, the department was active in developing new methodological approaches for the assessment of coronary haemodynamics before and after coronary interventions, using intra-coronary pressure and flow velocity measurements, acquired with sensor-tip guidewires[10].

Table 1. Literature on non-invasive FFR derivation.

First author	Year	Journal	Title
Patient-specific 3D blood flow analysis and treatment planning			
Taylor CA	1998	Computer Methods in Applied Mechanics and Engineering	Finite element modelling of blood flow in arteries
Taylor CA	1999	Computer Aided Surgery	Predictive medicine: Computational techniques in therapeutic decision-making
Validation of patient-specific blood flow analysis			
Ku JP	2002	Annals of Biomedical Engineering	In vivo validation of numerical prediction of blood flow in arterial bypass grafts
Ku JP	2005	Annals of Biomedical Engineering	Comparison of CFD and MRI flow and velocities in an in vitro large artery bypass graft model
Steele BN	2003	IEEE Transactions on Biomedical Engineering	In vivo validation of a one-dimensional finite-element method for predicting blood flow in cardiovascular bypass grafts
Steele BN	2007	Computer Methods in Biomechanics and Biomedical Engineering	Fractal network model for simulating abdominal and lower extremity blood flow during resting and exercise conditions
Anisotropic, adaptive and boundary layer mesh generation for cardiovascular flow			
Müller J	2005	Computer Methods in Biomechanics and Biomedical Engineering	Anisotropic adaptive finite element method for modelling blood flow
Sahni O	2006	Computer Methods in Applied Mechanics and Engineering	Efficient anisotropic adaptive discretisation of the cardiovascular system
Sahni O	2008	Engineering with Computers	Adaptive boundary layer meshing for viscous flow simulations
Sahni O	2009	Engineering with Computers	Automated adaptive cardiovascular flow simulations
Physiologically realistic outflow boundary conditions & Coupled blood flow-wall dynamics			
Vignon-Clementel IE	2006	Computer Methods in Applied Mechanics and Engineering	Outflow boundary conditions for three-dimensional finite element modelling of blood flow and pressure in arteries
Spilker RL	2010	Annals of Biomedical Engineering	Tuning multi-domain haemodynamic simulations to match physiological measurements
Figueroa CA	2006	Computer Methods in Applied Mechanics and Engineering	A coupled momentum method for modelling blood flow in three-dimensional deformable arteries
Vignon-Clementel IE	2010	Computer Methods in Biomechanics and Biomedical Engineering	Outflow boundary conditions for 3D simulations of non-periodic blood flow and pressure fields in deformable arteries
Direct 3D image segmentation and geometric modelling			
Bekkers EJ	2008	IEEE Transactions on Medical Imaging	Multiscale vascular surface model generation from medical imaging data using hierarchical features.
Xiong G	2011	International Journal for Numerical Methods in Biomedical Engineering	Simulation of blood flow in deformable vessels using subject-specific geometry and spatially varying wall properties
Development of methods for modelling coronary flow and auto-regulatory mechanisms			
Kim HJ	2009	Computer Methods in Applied Mechanics and Engineering	Augmented Lagrangian method for constraining the shape of velocity profiles at outlet boundaries for three-dimensional finite element simulations of blood flow
Kim HJ	2009	Annals of Biomedical Engineering	On coupling a lumped parameter heart model and a three-dimensional finite element aorta model
Kim HJ	2010	Finite Elements in Analysis and Design	Developing computational methods for three-dimensional finite element simulations of coronary blood flow
Kim HJ	2010	Annals of Biomedical Engineering	Patient-specific modeling of blood flow and pressure in human coronary arteries
Kim HJ	2010	Annals of Biomedical Engineering	Incorporating auto-regulatory mechanisms of the cardiovascular system in three-dimensional finite element models of arterial blood flow

3D: three-dimensional; CFD: computational fluid dynamics; FFR: fractional flow reserve; MRI: magnetic resonance imaging

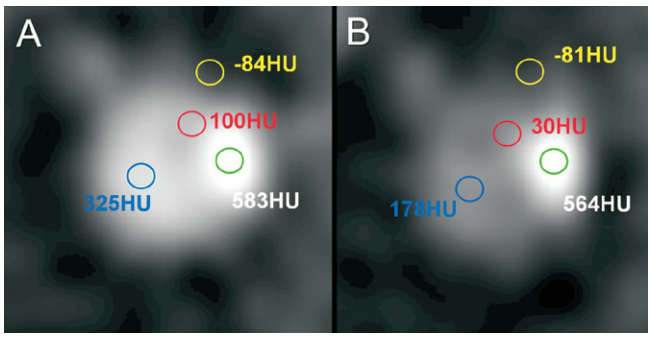

Figure 1. *Impact of luminal contrast density on plaque density measurements in multislice computed tomography (adapted from reference 4). The same coronary artery cross-section is shown at the time of peak contrast filling (A) and in the delayed phase of contrast enhancement (B). Whereas the density (in Hounsfield units, HU) does not change for either coronary calcium (green circle) or the surrounding epicardial fat (yellow), plaque density (red) is significantly decreased, as soon as the contrast medium is cleared out of the vessel lumen (blue).*

Fractional flow reserve

Fractional flow reserve (FFR), the ratio of maximal blood flow on either side of a coronary artery stenosis (distal vessel flow divided by proximal vessel flow), was introduced almost two decades ago[11], has been intensively validated and has demonstrated its clinical utility in deferring percutaneous treatment that would not have been appropriate in non-flow-limiting stenoses[12]. In clinical practice, beyond the temptation to treat unnecessarily (*ad hoc* on the table of the cathlab) a lesion that does not warrant percutaneous treatment, the (interventional) cardiologist is flooded with information derived from non-invasive angiography studies suggesting the presence of added coronary lesions next to the ones involved in the aetiology of an ischaemic event. In order to filter out the false positives (and taking into account the modest positive predictive value of CTA)[13], a multitude of non-invasive tests are performed and further developed to define anatomy, to determine the functional repercussions of narrowing on the blood flow, or to assess the myocardial sequelae of ischaemia[14-17]. The tests involve different disciplines of investigation (radio-nuclear, echocardiography, magnetic resonance imaging), and constitute a severe financial burden for society[18,19], and a substantial psychological nuisance for the patient submitted to this battery of diagnostic tests, sometimes redundant. The desire to have a single diagnostic modality providing all the information in one single non-invasive assessment is long awaited[20].

Non-invasive FFR assessment with MSCT

FFR_{CT} technology is based on three key underlying principles for the generation of physiologic models of coronary blood flow. According to the first principle, baseline coronary blood flow is met by myocardial demand for oxygen at rest. Allometric scaling laws of the form

$$Q_c^{rest} \propto M_{myo}^{k}$$

can be used to estimate physiological parameters: for instance, coronary flow (Q_c) under baseline conditions given an organ mass M_{myo}; k is the scaling factor[21-23]. Adherence to this principle enables calculation of total resting coronary blood flow relative to patient-specific left and right ventricular mass that can be quantified on the same MSCT scan. Naturally this assumption does not apply to patients with angina at rest and thus would prohibit analysis with FFR_{CT} technology in them. The second principle claims that the resistance of the microcirculatory vascular bed at rest is inversely, but not linearly, proportional to the size of the feeding vessel as demonstrated in prior morphometry, shear stress autoregulation, and compensatory remodelling research[24-30]. In other words, healthy and diseased blood vessels adapt to the amount of flow they carry. Power law relationships of the form

$$r_p^{k} = r_{d1}^{k} + r_{d2}^{k}$$

apply to the coronary arteries; autoregulation of wall shear stress provides the mechanism to explain observed power laws inherent in flow-diameter relationships[26,27]. The third principle says that the coronary microcirculation has a predictable response to adenosine, which is produced as soon as the heart lacks oxygen, with a breakdown of ATP, resulting in a release of adenosine. Exogenous administration of adenosine elicits the maximum hyperaemic responses by producing complete relaxation of the smooth muscle cells lining the resistance arterioles. Coronary flow reserve (ratio of flow during maximum hyperaemia to resting flow) is modulated by both epicardial and microcirculatory resistance[31]. This is based upon a prior landmark study by Wilson and colleagues, who identified a predictable response of the total coronary resistance to hyperaemia induction by intravenous or intracoronary administration of adenosine. What is most important with FFR_{CT} technology is that it does not require any modifications in coronary CTA acquisition protocols, additional imaging, or administration of additional medicine.

Cardiovascular computational fluid dynamics

Any application of computational fluid dynamics to structures as small as the coronary circulation bed requires unique capabilities for finite element mesh generation and modification[32]. A flow of an incompressible fluid, such as blood, submitted to a high driving pressure (e.g., 100 mmHg) could be highly accelerated when a small additional gradient of pressure is applied: this could generate significant changes in wall shear stress which require customised solving tools. Within current algorithms, finite element meshes can iteratively adapt their resolution in an anisotropic fashion, while the distribution of element size and density can be modified according to computation requirements[33,34]. Whereas in areas of less complex flow the mesh elements may be coarser and less dense, structured layers of elements are required near the vessel wall (boundary layers) in order to enhance the accuracy of wall shear stress computations, especially in exceedingly curved vessels[35]. On the other hand, flow-pressure variations in the coronary arteries cannot be directly measured as they are inherently part of the solution. Coronary flow distribution is modulated by both the resistance of the downstream vascular bed and the intra-myocardial pressure due to ventricular myocardium contraction[36]. Flow is not always proportional to pressure: thus, their relationship at the outlets of the coronaries is better expressed in the form of outflow boundary con-

ditions coupling the 3D epicardial domain to the microvasculature. Conversely, the influence of preload, heart rate, contractility and cardiac output can be modelled in appropriately set inflow boundary conditions[37].

Based upon the aforementioned three principles, a dedicated algorithm using cardiovascular computational flow dynamics was created (HeartFlow™; HeartFlow Inc., Redwood City, CA, USA) for non-invasive FFR derivation. The anatomy of the coronary arterial bed of a particular patient is not known *a priori* and has to be extracted from a patient-specific medical imaging dataset. MSCT can provide an accurate coronary geometric model, including branching and pathology specific to a patient. Based upon this geometric information, a volumetric finite element mesh with anisotropic refinement and boundary layers is generated in order to compute numerical results **(Figure 2)**. Using a proprietary algorithm the heart-vessel interaction can be defined, whereas time-varying coronary resistance for each coronary branch can be determined relative to intra-myocardial pressure and microvasculature impedance. This latter component can be represented by a so-called lumped (zero-dimensional) parameter model, which resembles an electric circuit, including resistive and capacitive elements **(Figure 3)**[36]. Finally the complex fluid properties of the blood are entered into the model, in order to refine the computations.

Upon completion of the blood flow analysis, mean coronary pressure is extracted from the computer analysis performed under maximum hyperaemic conditions. The FFR_{CT} is defined as the computed mean coronary pressure distal to a lesion divided by the computed mean blood pressure in the aorta under conditions of simulated maximum hyperaemia.

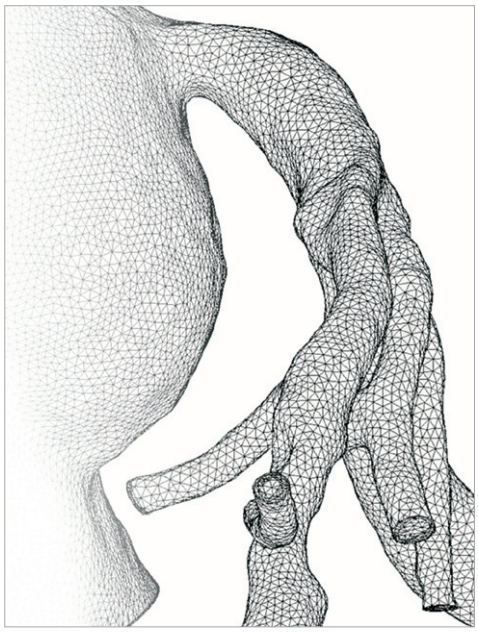

Figure 2. *Finite element model of a left coronary artery. The distribution of element size and density can be iteratively adapted to computation requirements.*

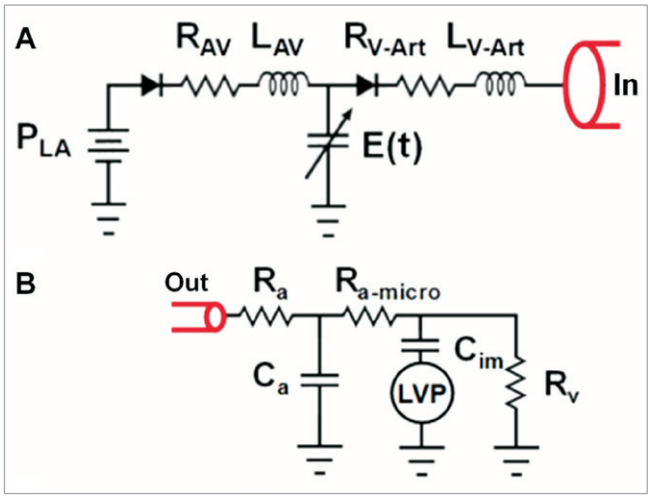

Figure 3. *Lumped (zero-dimensional) parameter models used in cardiovascular blood flow simulations. A) Lumped parameter heart model coupling the left heart side to the aortic inlet (In) of a closed loop system comprising the systemic and pulmonary circulation. The left heart side model consists of left atrial pressure P_{LA}, mitral valve, atrioventricular valvular resistance R_{AV}, atrioventricular inductance L_{AV}, aortic valve, ventriculo-arterial valvular resistance $R_{V\text{-}Art}$, ventriculo-arterial inductance $L_{V\text{-}Art}$, and left ventricular (LV) pressure. The LV pressure is modelled with time-varying LV elastance E(t). B) Lumped parameter coronary vascular bed model coupled to a coronary branch outlet (Out). This model consists of coronary arterial and venous resistance (R_a and R_v, respectively), coronary arterial microcirculation resistance $R_{a\text{-}micro}$, coronary arterial capacitance C_a, intramyocardial vascular capacitance C_{im}, and LV pressure; LV pressure stands for intra-myocardial pressure for branches perfusing the left ventricle and septum.*

The included moving image **(Moving image 1)** represents an actual measurement of FFR_{CT} provided by applying the basic scientific principles, as integrated in the proprietary algorithm briefly and succinctly described above. The customer has to upload the patient case onto a dedicated website: the very first step is segmentation of the major vessels, followed by plaque detection and removal, providing smooth luminal surfaces of the vascular bed. The model is trimmed and outflow boundaries are identified, and a patient-specific volumetric finite element mesh is generated and solved. Coronary blood flow and pressure are subsequently computed under conditions of maximal hyperaemia. On the moving image file, one can observe the luminogram of a left coronary artery as derived from the MSCT scan: particles flowing through the blood stream help visualise the vascular laminar flow proximal to a bifurcation (lesion) and the region of high velocity (in red on **Moving image 1**) with flow reversal and oscillatory shear stress immediately distal to it. In the left upper part of the movie, the pressure gradient is depicted whereas the FFR_{CT} value is continuously tracked on the coronary circulation, while scrolling from the distal vessel toward the main stem, where the FFR_{CT} gets normalised. The algorithm provides the option to perform virtual percutaneous coronary intervention (PCI) of the diseased

segment (by, for instance, virtually implanting a stent), and simulate the functional result of the treatment by re-calculating the FFR_{CT} values. Then the physician can choose from among a number of alternative treatment strategies and implement the one which would yield the best result.

The diagnostic performance of FFR_{CT} and coronary CTA-derived diameter stenosis (50% cut-off) compared to invasive FFR used as a reference standard has recently been reported in 159 vessels (103 patients)[38]; an FFR_{CT} ≤0.80 was considered diagnostic of lesion-specific ischaemia. Measurements for FFR_{CT} and FFR were highly correlated (coefficient=0.72, p<0.001), whereas FFR_{CT} slightly underestimated invasive FFR (mean difference 0.02±0.12, p=0.02). Accuracy, sensitivity, specificity, positive predictive value and negative predictive value of the FFR_{CT} and coronary CTA-derived diameter stenosis >50% are shown in **Figure 4**.

Over the past decade, non-invasive imaging using MSCT has lived up to its promises: luminography and tissue characterisation have made major progress in quantification, due to continuous increase in spatial (16, 64, 128, 256 and 320 detectors/slices) and temporal resolution, despite some inherent limitations of x-ray regarding tissue characterisation. The adjunction of functional assessment for flow-limiting lesions is a quantum leap in the non-invasive evaluation of patients prior to PCI with the option of virtual treatment planning. Consequently, a single MSCT study will ultimately provide us with comprehensive "one-stop" non-invasive evaluation of the coronaries.

Examples of clinical cases

CASE 1

The first clinical example concerns a patient who five years ago received a bioresorbable everolimus-eluting scaffold in the proximal right coronary artery (RCA). At 6-month and 24-month follow-up, the conventional angiography did not show any significant stenosis in the scaffolded segment. At five-year follow-up, the MSCT scan showed a patent, non-stenotic scaffolded area demarcated by the two radiopaque platinum markers (black arrows, **Figure 5**). On the maximum intensity projection, two small calcified plaques are visible distal to the scaffold. Non-invasive functional assessment showed that all three vessels exhibited distally FFR_{CT} values above a threshold of 0.80: specifically, there was no gradient in FFR_{CT} along the scaffolded segment.

CASE 2

The second case concerns a patient with obstructive disease in the proximal left anterior descending (LAD) coronary artery, causing ischaemia in both LAD and the first diagonal branch (D1). Disease extends from the proximal LAD to the take-off of the first septal branch. Using the computer models based on non-invasive FFR derivation **(Figure 6)**, one could describe this anatomy as a Medina (1,0,0) lesion at the LAD-D1 bifurcation plus one separate distal LAD lesion just proximal to the take-off of the septal branch. Alternatively, one could describe two sequential (1,0,0) bifurcation lesions, if the septal is considered to be a major vessel and therefore warrants protection. Following these diagnostic considerations, the treatment plan could be shaped accordingly. In the latter diagnostic approach, one could consider a provisional T-stent procedure for the diagonal branch with guidewire protection for the septal branch. On the other hand, if the septal is perceived to be a small vessel, one could opt for a culotte approach using a Tryton Side-Branch Stent™ (Tryton Medical, Inc., Newton, MA, USA), provided that the distance between the ostium of the circumflex and the ostium of the first diagonal is compatible with the length of the proximal part of the Tryton stent; subsequently, a long drug-eluting stent would be placed in the LAD, possibly covering the ostium of the septal branch.

CASE 3

The last case concerns a 65-year-old male patient with stable angina: his coronary risk factors were hypertension and hypercholesterolaemia. MSCT angiography disclosed two stenotic lesions,

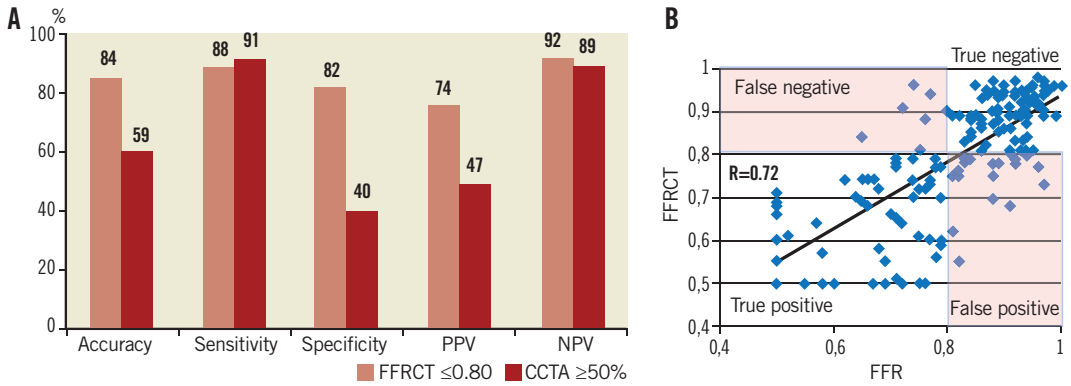

Figure 4. *Diagnostic performance of FFR_{CT} compared to invasive FFR in 159 vessels[38]. A) Accuracy, sensitivity, specificity, positive and negative predictive value (PPV and NPV, respectively) for FFR_{CT} and CCTA-derived diameter stenosis (50% cut-off). B) Correlation of FFR_{CT} with invasive FFR values was high (R=0.72, p<0.001). A cut-off of ≤0.80 was considered diagnostic of lesion-specific ischaemia for both FFR_{CT} and FFR. CCTA: coronary CT angiography; FFR: fractional flow reserve*

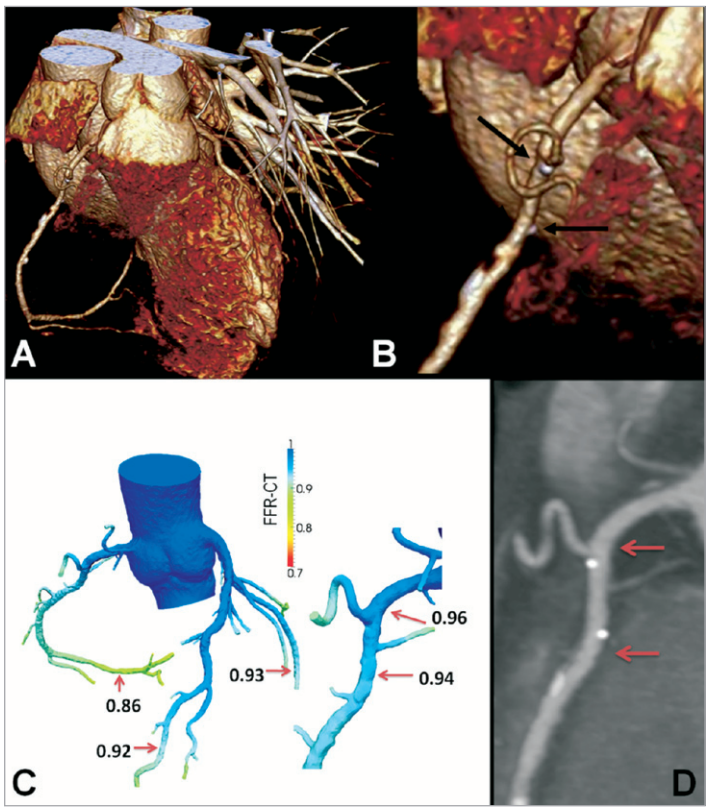

Figure 5. *Use of non-invasive FFR for follow-up of a bioresorbable scaffold. A) Three-dimensional volume-rendered CT angiogram of a right coronary artery. Magnification of the proximal artery segment (B) shows the platinum markers of the resorbed scaffold (black arrows). C) Non-invasive FFR derivation did not show ischaemia in any coronary artery. Specifically, FFR_{CT} measured 0.96 and 0.94 at the inflow and outflow of the scaffolded segment (red arrows on the curved multi-planar CT image) (D). The colour scale of the CCTA-derived computer models is based on the FFR_{CT} values. CCTA: coronary CT angiography; FFR: fractional flow reserve*

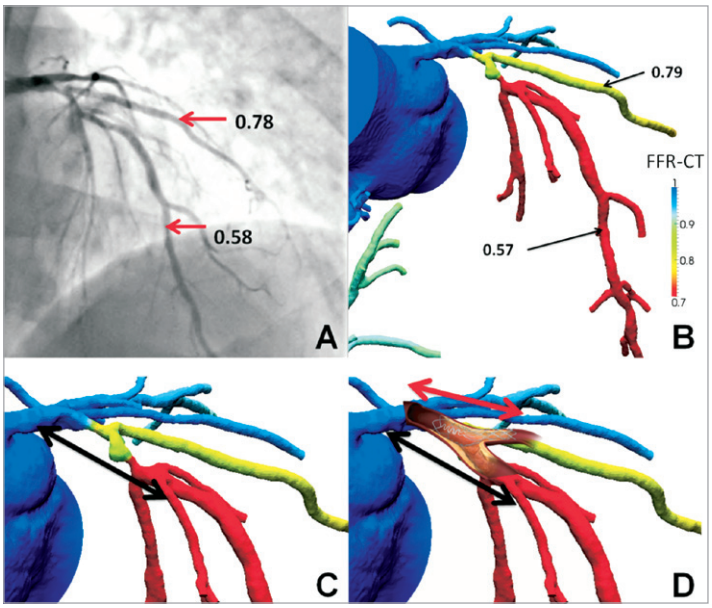

Figure 6. *Use of non-invasive FFR in procedural strategy for bifurcation PCI. Proximal LAD disease causes ischaemia in both the distal LAD and first diagonal branch (D1); invasive (A) and non-invasive estimates (B) are concordant. The colour coding of the computer models facilitates ischaemia localisation. Dependent on diagnostic interpretation (including the size of the first septal branch), either a provisional T-stent (C) or a Culotte approach using a Tryton Side-Branch Stent™ (D) can be followed. The black arrows indicate the position where the drug-eluting stent will be placed in the proximal LAD. FFR: fractional flow reserve; LAD: left anterior descending coronary artery*

one in the ostium of the LAD and one in the mid portion of the RCA, respectively (not shown). The mid to distal LAD had a FFR_{CT} of 0.71 vs. 0.74 with the invasive approach **(Figure 7)**. Left main stem (LM) anatomy could be interpreted as either a trifurcation with one vessel segment diseased (LAD ostium), hence a Medina (0,1,0,0) lesion or as a trifurcation with two diseased vessel segments (also involving the LM), therefore a (1,1,0,0) lesion. Irrespective of diagnostic interpretation, one would consider stenting the mid intermediate branch lesion without touching the trifurcation. Nevertheless, according to interpretation one could consider treating the LAD ostium alone, or alternatively place a stent from the LM into the proximal LAD with a provisional 2-3 stent strategy. Virtual PCI of the LAD ostium alone resulted in a limited improvement, FFR_{CT} slightly increasing from 0.77 to 0.80. The most striking observation was a drop in FFR_{CT} along the LM measuring 0.81 in its mid portion. Virtual treatment of LM alone already normalised FFR_{CT} in the mid LAD (FFR_{CT}=0.90). The combined treatment of LM and LAD ostium resulted in further improvement of the FFR_{CT} up to a value of 0.93.

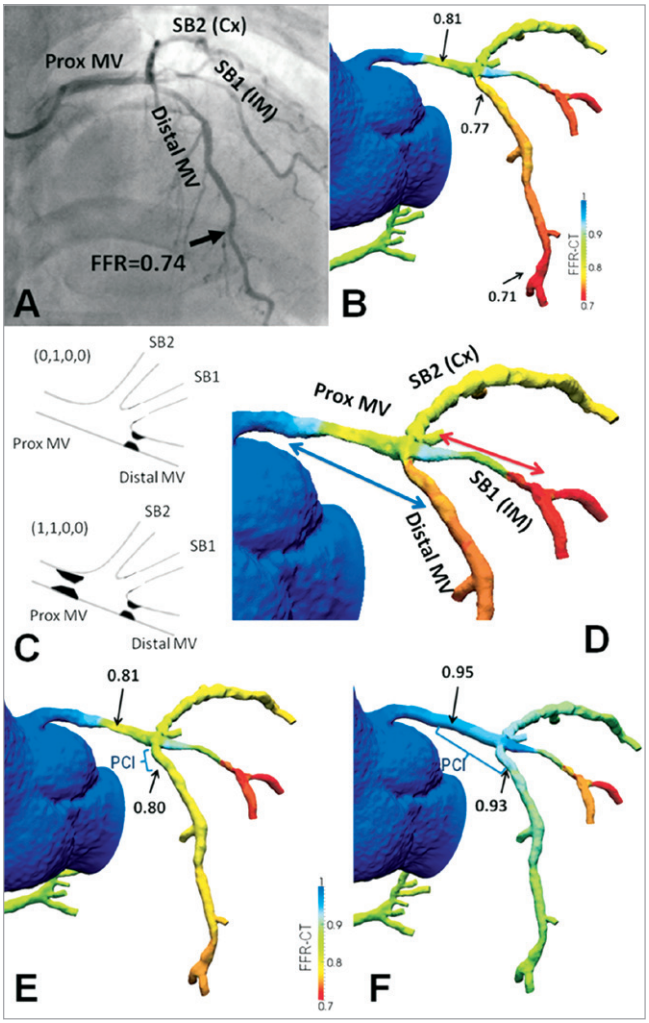

Figure 7. *The yield of virtual treatment planning with non-invasive FFR measurements in an ambiguous left main (LM) stem anatomy. Both invasive (A) and non-invasive FFR estimates (B) showed ischaemia in the mid-distal LAD. According to diagnostic interpretation (see case description) (C) one can opt for treating the LAD ostium alone or place a stent from the LM into the proximal LAD (blue arrow) (D). The former option does not fully alleviate ischaemia (E), whereas the latter one does (F). Cx: (left) circumflex coronary artery; FFR: fractional flow reserve; IM: intermediate (branch); LAD: left anterior descending coronary artery; MV: main vessel; PCI: percutaneous coronary intervention; SB: side branch*

Acknowledgements

The authors would like to acknowledge the contribution of Charles A. Taylor, PhD and John H. Stevens (HeartFlow Inc., Redwood City, CA, USA) regarding the description of HeartFlow™ technology and the analysis of clinical case examples as well as Bon Kwon Koo (Seoul National University Hospital, Seoul, South Korea) and James K. Min (Cedars-Sinai Heart Institute, Los Angeles, CA, USA) for providing cases 2 and 3 from the DISCOVER-FLOW population.

Glossary

allometry: change in proportion of various parts of an object/organism as a consequence of growth

anisotropy: the property of being directionally dependent. An example of an anisotropic material is wood, which is easier to split along its grain than against it

impedance: frequency analogue of resistance

lumped (model): zero-dimensional model

Conflict of interest statement

The authors have no conflicts of interest to declare.

References

1. Otsuka M, Bruining N, Van Pelt NC, Mollet NR, Ligthart JM, Vourvouri E, Hamers R, De Jaegere P, Wijns W, Van Domburg RT, Stone GW, Veldhof S, Verheye S, Dudek D, Serruys PW, Krestin GP, De Feyter PJ. Quantification of coronary plaque by 64-slice computed tomography: a comparison with quantitative intracoronary ultrasound. *Invest Radiol.* 2008;43:314-21.

2. Voros S, Rinehart S, Qian Z, Vazquez G, Anderson H, Murrieta L, Wilmer C, Carlson H, Taylor K, Ballard W, Karmpaliotis D, Kalynych A, Brown C, 3rd. Prospective validation of standardized, 3-dimensional, quantitative coronary computed tomographic plaque measurements using radiofrequency backscatter intravascular ultrasound as reference standard in intermediate coronary arterial lesions: results from the ATLANTA (assessment of tissue characteristics, lesion morphology, and hemodynamics by angiography with fractional flow reserve, intravascular ultrasound and virtual histology, and noninvasive computed tomography in atherosclerotic plaques) I study. *JACC Cardiovasc Interv.* 2011;4:198-208.

3. Cademartiri F, Mollet NR, Runza G, Bruining N, Hamers R, Somers P, Knaapen M, Verheye S, Midiri M, Krestin GP, de Feyter PJ. Influence of intracoronary attenuation on coronary

plaque measurements using multislice computed tomography: observations in an ex vivo model of coronary computed tomography angiography. *Eur Radiol.* 2005;15:1426-31.

4. Cademartiri F, Runza G, Palumbo A, Maffei E, Martini C, McFadden E, Somers P, Knaapen M, Verheye S, Weustink AC, Mollet NR, de Feyter PJ, Hamers R, Bruining N. Lumen enhancement influences absolute noncalcific plaque density on multislice computed tomography coronary angiography: ex-vivo validation and in-vivo demonstration. *J Cardiovasc Med* (Hagerstown). 2010;11:337-44.

5. Sun J, Zhang Z, Lu B, Yu W, Yang Y, Zhou Y, Wang Y, Fan Z. Identification and quantification of coronary atherosclerotic plaques: a comparison of 64-MDCT and intravascular ultrasound. *AJR Am J Roentgenol*. 2008;190:748-54.

6. Motoyama S, Sarai M, Harigaya H, Anno H, Inoue K, Hara T, Naruse H, Ishii J, Hishida H, Wong ND, Virmani R, Kondo T, Ozaki Y, Narula J. Computed tomographic angiography characteristics of atherosclerotic plaques subsequently resulting in acute coronary syndrome. *J Am Coll Cardiol*. 2009;54:49-57.

7. Rinehart S, Vazquez G, Qian Z, Murrieta L, Christian K, Voros S. Quantitative measurements of coronary arterial stenosis, plaque geometry, and composition are highly reproducible with a standardized coronary arterial computed tomographic approach in high-quality CT datasets. *J Cardiovasc Comput Tomogr*. 2011;5:35-43.

8. Wentzel JJ, van der Giessen AG, Garg S, Schultz C, Mastik F, Gijsen FJ, Serruys PW, van der Steen AF, Regar E. In vivo 3D distribution of lipid-core plaque in human coronary artery as assessed by fusion of near infrared spectroscopy-intravascular ultrasound and multislice computed tomography scan. *Circ Cardiovasc Imaging*. 2010;3:e6-7.

9. Slager CJ, Wentzel JJ, Schuurbiers JC, Oomen JA, Kloet J, Krams R, von Birgelen C, van der Giessen WJ, Serruys PW, de Feyter PJ. True 3-dimensional reconstruction of coronary arteries in patients by fusion of angiography and IVUS (ANGUS) and its quantitative validation. *Circulation*. 2000;102:511-16.

10. Serruys PW, Di Mario C, Meneveau N, de Jaegere P, Strikwerda S, de Feyter PJ, Emanuelsson H. Intracoronary pressure and flow velocity with sensor-tip guidewires: a new methodologic approach for assessment of coronary hemodynamics before and after coronary interventions. *Am J Cardiol.*1993;71:41D-53D.

11. Pijls NH, van Son JA, Kirkeeide RL, De Bruyne B, Gould KL. Experimental basis of determining maximum coronary, myocardial, and collateral blood flow by pressure measurements for assessing functional stenosis severity before and after percutaneous transluminal coronary angioplasty. *Circulation*. 1993;87:1354-67.

12. Pijls NH, van Schaardenburgh P, Manoharan G, Boersma E, Bech JW, van't Veer M, Bar F, Hoorntje J, Koolen J, Wijns W, de Bruyne B. Percutaneous coronary intervention of functionally nonsignificant stenosis: 5-year follow-up of the DEFER Study. *J Am Coll Cardiol*. 2007;49:2105-11.

13. Schroeder S, Achenbach S, Bengel F, Burgstahler C, Cademartiri F, de Feyter P, George R, Kaufmann P, Kopp AF, Knuuti J, Ropers D, Schuijf J, Tops LF, Bax JJ. Cardiac computed tomography: indications, applications, limitations, and training requirements: report of a Writing Group deployed by the Working Group Nuclear Cardiology and Cardiac CT of the European Society of Cardiology and the European Council of Nuclear Cardiology. *Eur Heart J*. 2008;29:531-56.

14. Underwood SR, Bax JJ, vom Dahl J, Henein MY, Knuuti J, van Rossum AC, Schwarz ER, Vanoverschelde JL, van der Wall EE, Wijns W. Imaging techniques for the assessment of myocardial hibernation. Report of a Study Group of the European Society of Cardiology. *Eur Heart J.* 2004;25:815-36.

15. Berman DS, Hachamovitch R, Shaw LJ, Friedman JD, Hayes SW, Thomson LE, Fieno DS, Germano G, Wong ND, Kang X, Rozanski A. Roles of nuclear cardiology, cardiac computed tomography, and cardiac magnetic resonance: Noninvasive risk stratification and a conceptual framework for the selection of noninvasive imaging tests in patients with known or suspected coronary artery disease. *J Nucl Med*. 2006;47:1107-18.

16. Di Carli MF, Hachamovitch R. New technology for noninvasive evaluation of coronary artery disease. *Circulation*. 2007;115:1464-80.

17. Salerno M, Beller GA. Noninvasive assessment of myocardial perfusion. *Circ Cardiovasc Imaging*. 2009;2:412-24.

18. Min JK, Hachamovitch R, Rozanski A, Shaw LJ, Berman DS, Gibbons R. Clinical benefits of noninvasive testing: coronary computed tomography angiography as a test case. *JACC Cardiovasc Imaging*. 2010;3:305-15.

19. Schoenhagen P, Hachamovitch R, Achenbach S. Coronary CT angiography and comparative effectiveness research prognostic value of atherosclerotic disease burden in appropriately indicated clinical examinations. *JACC Cardiovasc Imaging*. 2011;4:492-5.

20. Williams MC, Reid JH, McKillop G, Weir NW, van Beek EJ, Uren NG, Newby DE. Cardiac and coronary CT comprehensive imaging approach in the assessment of coronary heart disease. *Heart.* 2011;97:1198-205.

21. West GB, Brown JH, Enquist BJ. A general model for the origin of allometric scaling laws in biology. *Science*. 1997;276:122-26.

22. Steele BN, Olufsen MS, Taylor CA. Fractal network model for simulating abdominal and lower extremity blood flow during resting and exercise conditions. *Comput Methods Biomech Biomed Engin*. 2007;10:39-51.

23. Choy JS, Kassab GS. Scaling of myocardial mass to flow and morphometry of coronary arteries. *J Appl Physiol*. 2008;104:1281-6.

24. Murray CD. The Physiological Principle of Minimum Work: I. The Vascular System and the Cost of Blood Volume. Proc Natl Acad Sci U S A. 1926; 12:207-14.

25. Hutchins GM, Miner MM, Boitnott JK. Vessel caliber and branch-angle of human coronary artery branch-points. *Circ Res*. 1976;38:572-76.

26. Kamiya A, Togawa T. Adaptive regulation of wall shear stress to flow change in the canine carotid artery. *Am J Physiol.* 1980;239:H14-21.

27. Zarins CK, Zatina MA, Giddens DP, Ku DN, Glagov S. Shear stress regulation of artery lumen diameter in experimental atherogenesis. *J Vasc Surg.* 1987;5:413-20.

28. LaBarbera M. Principles of design of fluid transport systems in zoology. *Science.* 1990;249:992-1000.

29. Zhou Y, Kassab GS, Molloi S. On the design of the coronary arterial tree: a generalization of Murray's law. *Phys Med Biol*. 1999; 44:2929-45.

30. Zhou Y, Kassab GS, Molloi S. In vivo validation of the design rules of the coronary arteries and their application in the assessment of diffuse disease. *Phys Med Biol*. 2002;47:977-93.

31. Wilson RF, Wyche K, Christensen BV, Zimmer S, Laxson DD. Effects of adenosine on human coronary arterial circulation. *Circulation.* 1990;82:1595-606.

32. Kim HJ, Vignon-Clementel IE, Figueroa CA, Jansen KE, Taylor CA. Developing computational methods for three-dimensional finite element simulations of coronary blood flow. *Finite Elements in Analysis and Design*. 2010;46:514-25.

33. Müller J, Sahni O, Li X, Jansen KE, Shephard MS, Taylor CA. Anisotropic adaptive finite element method for modelling blood flow. *Comput Methods Biomech Biomed Engin.* 2005;8:295-305.

34. Sahni O, Müller J, Jansen KE, Shephard MS, Taylor CA. Efficient anisotropic adaptive discretization of the cardiovascular system. *Comput Methods Appl Mech Engrg*. 2006;195:5634-55.

35. Sahni O, Jansen KE, Taylor CA, Shephard MS. Automated adaptive cardiovascular flow simulations. *Engineering with Computers*. 2009;25:25-36.

36. Kim HJ, Vignon-Clementel IE, Coogan JS, Figueroa CA, Jansen KE, Taylor CA. Patient-specific modeling of blood flow and pressure in human coronary arteries. *Ann Biomed Eng*. 2010;38: 3195-209.

37. Kim HJ, Vignon-Clementel IE, Figueroa CA, LaDisa JF, Jansen KE, Feinstein JA, Taylor CA. On coupling a lumped parameter heart model and a three-dimensional finite element aorta model. *Ann Biomed Eng*. 2009;37:2153-69.

38. Koo BK, Erglis A, Doh JH, Daniels DV, Jegere S, Kim HS, Dunning A, Defrance T, Lansky A, Leipsic J, Min JK. Diagnosis of Ischemia-Causing Coronary Stenoses by Noninvasive Fractional Flow Reserve Computed From Coronary Computed Tomographic Angiograms Results From the Prospective Multicenter DISCOVER-FLOW (Diagnosis of Ischemia-Causing Stenoses Obtained Via Noninvasive Fractional Flow Reserve) Study. *J Am Coll Cardiol*. 2011;58:1989-97.

Online data supplement

Moving image 1. Example of FFR_{CT} measurements including virtual treatment.